Next Materials 3 (2024) 100094

Contents lists available at ScienceDirect

Next Materials

journal homepage: www.sciencedirect.com/journal/next-materials

Research article

New insights on the role of perimeter sites in oxygen and methanol activation during furfural oxidative esterification over gold supported catalysts

M. Manzoli [a,*], F. Menegazzo [b], M. Belluati [a], E. Calcio Gaudino [a], S. Tabasso [a], M. Signoretto [b]

[a] Department of Drug Science and Technology and NIS Centre, University of Turin, Via P. Giuria 9, 10125 Turin, Italy
[b] Department of Molecular Sciences and Nanosystems, Ca' Foscari University Venice and INSTM-RU Ve, Via Torino 155, 30170 Venezia Mestre, Italy

ARTICLE INFO

Keywords:
Gold catalyst
Zirconia
Furfural oxidative esterification
Oxygen activation, methanol activation, Au perimeter sites

ABSTRACT

Au/ZrO_2 catalysts (1.5 wt% Au loading) undergone to a final calcination at different temperature (423, 573, 773 and 923 K) to opportunely modulate the Au size were proven to be highly active and selective in furfural oxidative esterification to methyl-2-furoate. The catalysts were tested according to previously optimized reaction conditions, employing O_2 as benign oxidant and without any base co-catalyst. The strong dependence of the catalytic activity on the Au size was previously ascribed to the presence of Au clusters able to dissociate O_2 and producing atomic O that can activate methanol. However, despite the absence of clusters, also the catalysts containing larger Au nanoparticles were active, even if conversion and selectivity were remarkably lower if compared to the other samples. The nature and the role of Au active sites exposed at the surface of clusters and nanoparticles were then investigated by HR-TEM, CO chemisorption and FTIR spectroscopy of adsorbed CO, molecular oxygen, methanol and furfural to establish structure-activity relationships. Metal nanoparticles can activate oxygen and form superoxo species and atomic O, whereas experiments performed on the pre-hydrated samples revealed that Au perimeter sites at the metal-support interface play a key role in methanol activation during furfural oxidative esterification.

1. Introduction

The depletion of non-renewable fossil fuels boosted the research towards the exploitation of renewable and sustainable resources [1,2]. In the forthcoming concept of bio-refinery, the possibility to convert lignocellulosic biomass wastes into higher added-value chemicals is one of the most challenging approaches, because platform chemicals can be converted into compounds replacing those coming from petrol chemistry. Among platform chemicals, furfural (2-FA) has been recognized by the U.S. Department of Energy as one of the top 12 biomass-derived platform carbohydrate compounds [3]. 2-FA is employed in the preparation of drugs, pesticides, paints, plastics, commodities and fine chemicals, solvents etc. [4], resulting in an increasing demand of its derivatives at a compound annual growth rate (CAGR) of 2.69%, with a production expected to achieve 1172.17 kt by 2024 [5]. Methyl 2-furoate is a 2-FA derivative that finds application in fine chemicals, flavor and fragrance industries and marine paints as antifoulants [6,7]. The conventional method to obtain this molecule involves the use of strong oxidizing agents, such as $KMnO_4$ to convert 2-FA to 2-furoic acid, which is then esterified by concentrated sulphuric acid in alcohol. Conversely, another method requires strong bases such as NaOH, K_2CO_3, Li_2CO_3, $CsCO_3$ etc. [8,9]. However, to be regarded as both economically attractive and sustainable, a process has to be carried out avoiding the use of non-corrosive reagents and harsh reaction conditions. With this in mind, the one-pot oxidative esterification of 2-FA to methyl 2-furoate, in which methanol is either reactant or solvent, is a promising green alternative, since it can be performed in the presence of molecular oxygen and of a suitable heterogeneous catalyst to prevent the use of any strong base [10,11]. Nevertheless, the number of attempts to carry out this reaction without using bases is still low [12–17]. As for the heterogeneous catalyst, many supported metals (as Au, Pd, Ag, Co) as well as bimetallic catalysts have been employed for oxidative esterification reactions [11,18–25]. In this frame, catalysis by gold became of increasing interest for reactions involving selective alcohol oxidations [26,27] as well as oxidative-coupling reactions [28]. Au catalysis in aerobic oxidation of alcohols and aldehydes has been also investigated

* Corresponding author.
E-mail address: maela.manzoli@unito.it (M. Manzoli).

https://doi.org/10.1016/j.nxmate.2023.100094
Received 17 July 2023; Received in revised form 12 December 2023; Accepted 14 December 2023
Available online 27 December 2023

in highly basic aqueous mediums [29–31].

The comprehension of the mechanism of alcohol activation on gold systems represents a crucial step in the study of the reactivity displayed by gold in several reactions. Over Au/ZnO, methanol dissociation has been reported to occur over the support, where methoxy species are formed and react with oxygen activated at the perimeter sites of the gold particles at the interface between the metal and the oxide [32]. On the contrary, formate species strongly bounded on the support are produced and act as poison for the Au/TiO_2 catalyst [32]. It was also reported that reactive methoxy species adsorbed on top on highly uncoordinated titanium sites, close to oxygen vacancies and uncoordinated gold sites are involved in methanol decomposition at low temperature [33]. Moreover, the methanol molecule reacts with the surface OH groups of the support producing methoxy species by elimination of water molecules already at room temperature and an effect of the nature of the support on methanol dissociation was found [34]. The enhanced activity in the 2-FA esterification to methyl furoate displayed by Au/ZrO_2 catalysts was ascribed to the presence of Au clusters able to dissociate O_2 producing atomic O with basic properties able to activate methanol [12]. It was also proposed that when supported on zirconia, Au nanoparticles should have size < 3 nm to be active in the reaction [35]. Moreover, it was unexpectedly found that the larger is the size of the Au nanoparticles supported on CeO_2, the higher is the activity in 2-FA esterification under the same experimental conditions [36]. It was finally shown that 2-FA took part to the reaction by interacting mainly with its carbonyl group with the catalyst surface [14]. Very recently Delparish *et al.* by ab initio density functional theory calculations proposed that in the reaction pathway O_2 regenerates the active sites by abstracting hydrogen from the Au surface, whereas methanol decomposes to form methoxy species over gold sites. It was also found that methanol decomposition was crucial to determine the overall reaction rate and to lower the amount of the additive base. Conversely, neither furfural nor the silica support participate in the rate-determining step of the reaction [37]. These results support on one hand, that there is a strong dependence of the catalytic performances from the nature of the support and the metal particle size, which affects the nature of the Au sites involved in the reaction and, on the other hand, that the final calcination temperature to which the samples underwent during preparation must be carefully controlled to obtain a gold active phase with tailored size.

In this study, FTIR spectroscopy of adsorbed CO, O_2, methanol and furfural coupled with HR-TEM analysis, as well as CO chemisorption and DR UV-Vis-NIR spectroscopy have been employed with the aims to investigate (i) the nature of the Au sites depending on the particle size, (ii) on which sites oxygen is activated, (iii) their role in methanol activation during 2-FA oxidative esterification and (iv) on which sites furfural is adsorbed. A series of tailored Au/ZrO_2 catalysts with the same metal loading (1.5 wt% Au) has been prepared. The samples have been submitted to different final calcination at different temperatures (from 423 up to 923 K) to obtain catalysts with modulated gold size and tested in the 2-FA oxidative esterification under previously optimized conditions [35] to establish structure-activity relationships.

2. Materials and methods

2.1. Preparation of the catalysts

The zirconia support was prepared by precipitation from the $ZrOCl_2{\cdot}8\ H_2O$ precursor at constant pH= 8.6, aged for 20 h at 363 K, washed, and dried at 383 K overnight. It was found that the addition of sulphates to zirconia promotes gold dispersion [38]. Therefore, to achieve a 2 wt% amount of sulphates on the final support, the obtained zirconium hydroxide was sulphated with $(NH_4)_2SO_4$ (Merck) by incipient wetness impregnation. Then the sulphated $Zr(OH)_4$ was then calcined in air at 923 K to get sulphated ZrO_2. Finally, gold (1.5 wt% loading) was added by deposition-precipitation to zirconia (5 g) suspended in 200 mL of an aqueous solution of $HAuCl_4{\cdot}3\ H_2O$ for 3 h at controlled pH= 8.6. The pH was kept constant by adding NaOH (0,5 M). The gold amount was determined by atomic adsorption spectroscopy. In this case, 100 mg of catalyst previously dried have been dissolved in an aqueous solution of HF and aqua regia and disaggregated under microwave irradiation. The actual gold loading is 1.5 wt%. After filtration, the samples were dried at 308 K overnight and finally calcined in air for 1 h at different temperature (423 K, 573 K, 773 K and 923 K) to modulate the size of the Au nanoparticles given the same Au loading. The catalysts were labelled as AuZ423, AuZ573, AuZ773 and AuZ923, respectively.

2.2. Characterization of the catalysts

High resolution transmission electron microscopy (HR-TEM) analyses were performed by using a 300 kV JEOL 3010-UHR microscope equipped with a LaB_6 filament and with X-ray EDS analysis by a Link ISIS 200 detector. Digital micrographs were acquired by a (2k x 2k)-pixel Ultrascan 1000 CCD camera and were processed by Gatan digital micrograph. For the analyses, the samples in the form of powders were contacted with a lacey carbon Cu grid, which resulted in the adhesion of the sample particles by electrostatic interaction, hence guaranteeing good dispersion of the particles on the grid and avoiding any modification induced using a solvent. Histograms of the Au particle size distributions were obtained by counting a representative number of particles for each sample and the mean particle diameter (d_m) was calculated by the following equation: $d_m = \Sigma d_i n_i / \Sigma n_i$ (n_i is the number of particles with diameter d_i). Au nanoparticles appeared well contrasted with respect to the zirconia support and the counting was performed on electron micrographs obtained starting from 300,000 × magnification. Based on each particle size distribution, the corresponding metal Specific Surface Area (SSA, m^2/g) of the Au nanoparticles (supposed to be hemispherical) was calculated by the equation: $3\Sigma n_i r_i^2 / (\delta_{Au} \Sigma n_i r_i^3)$ m^2/g (r_i is the mean radius of the size class containing n_i particles, and δ_{Au} the volumetric mass of Au, equal to 19.32 g/cm^3).

CO pulse chemisorption measurements on Au were performed at 157 K by using a lab-made equipment. Before the analyses the samples (200 mg) were reduced in a H_2 flow (40 mL/min) at 423 K for 60 min, cooled in H_2 to room temperature (r.t.), purged in He flow (40 mL/min) and hydrated at room temperature in a He flow (10 mL/min) saturated with a proper amount of water to avoid CO chemisorption on the support and therefore delete the contribution of the support. Then the samples were cooled in He flow to 157 K [39].

Diffuse reflectance UV–Vis-NIR (DR UV-Vis-NIR) analyses of the as prepared catalysts were performed in air at r.t. on a Varian Cary 5000 spectrophotometer, working in the 190–2500 nm range. The spectra of the reduced samples were collected in a cell allowing thermal treatments in controlled atmosphere and temperature. The AuZ423 and AuZ923 catalyst were submitted to a thermal pre-treatment in O_2 atmosphere followed by reduction in H_2 atmosphere. The activation procedure was chosen accordingly to the final calcination to which each sample underwent during preparation. The oxidation pre-treatment (deg./ox. procedure, the label is followed by the temperature of the pre-treatment) was performed as follows: heating from r.t. to 423 K under degassing; followed by an inlet of O_2 (20 mbar) and heating up to 423 K as for AuZ423 and 673 K for AuZ923, changing the oxygen atmosphere three times (20 mbar for 10 min each one) at the given temperature. The sample was then cooled down to r.t. in O_2 and finally degassed at the same temperature. For both catalysts, the reductive treatment was carried out (after oxidation) by heating from r.t. up to 423 K in H_2 (10 mbar), keeping that temperature for 10 min, then the sample was cooled to r.t. under outgassing (red./deg. procedure, the label is followed by the temperature of the reduction pre-treatment). The pre-treatment procedures to which the catalysts have been submitted before the DR UV-Vis-NIR and experiments are summarised in Table SM-1. UV–Vis-NIR spectra were reported in the Kubelka-Munk function [$f(R_\infty) = (1 - R_\infty)^2 / 2\ R_\infty$; R_∞=reflectance of an "infinitely thick" layer of the sample.

FTIR spectra were taken on a Bruker IFS66 spectrometer (equipped with a MCT detector) with the samples in self-supporting pellets introduced in a cell allowing thermal treatments in controlled atmospheres and spectrum scanning at controlled temperatures (from 90 to 300 K). From each spectrum, the background before the inlet of the probe was subtracted. All spectra have been normalised to the weight of the pellets. Before the FTIR experiments, the catalysts underwent to a thermal pre-treatment in O_2 atmosphere to clean the surface from water and carbonate-like species followed by reduction in H_2 atmosphere to obtain reduced gold sites. Also in this case, the detailed experimental conditions of the activation procedure were chosen accordingly to the final calcination to which each sample was submitted during preparation. In particular, the oxidative treatment (deg./ox. procedure, the label is followed by the temperature of the pre-treatment) included heating from r.t. to 423 K under degassing; followed by an inlet of O_2 (20 mbar) and heating up to 423 K as for AuZ423, 453 K in the case of AuZ573, and 673 K (AuZ773 and AuZ923). The O_2 was then changed three times (20 mbar for 10 min each one) at the given temperature. The sample was then cooled down to r.t. in oxygen and finally degassed at the same temperature. For all samples, the reductive treatment was carried out (after oxidation) by heating from r.t. up to 423 K in H_2 (10 mbar), keeping that temperature for 10 min. After that, the sample was cooled to r.t. under outgassing (red./deg. procedure, the label is then followed by the temperature of the reduction pre-treatment). Moreover, as for the experiments carried out with the methanol probe, the pre-treated catalysts were further pre-hydrated at r.t. (5 mbar H_2O for 60 min, then degassing to 2.5 $\times 10^{-2}$ mbar) to eliminate the contribution by the sites of the support before the exposure to the CO probe. As for the experiment on furfural interaction at r.t., the spectra were collected after the inlet of 20 mbar CO at r.t. on the AuZ573 catalyst (i) after the oxidative treatment (deg./ox. 573 K) followed by the reductive treatment (red./deg. 423 K), and (ii) after furfural adsorption (1 mbar) at r.t. and outgassing at the same temperature. The pre-treatment procedures to which the catalysts have been submitted before the FTIR experiments are summarised in Table SM-2.

2.3. Catalytic activity tests

2-FA esterification with O_2 and CH_3OH was investigated in previously optimized conditions (393 K, no $NaHCO_3$ addition, a batch reactor) [35]. Briefly, the Au/ZrO_2 catalyst (100 mg), 2-FA (Sigma Aldrich, >99%; 300 μL) and n-octane (internal standard, Sigma Aldrich, >99%; 150 μL) were added to CH_3OH (150 mL), which is reactant and solvent, choosing a Au/2-FA/CH_3OH molar ratio equal to 1/5 $\times$ 10^3/5 $\times$ 10^6. The reactor was charged with 12 bar O_2 under stirring at 1000 rpm. GC analysis of the converted mixture was performed after 180 min (capillary column HP-5, FID detector). The kinetic studies were carried out after 15, 40 and 90 min

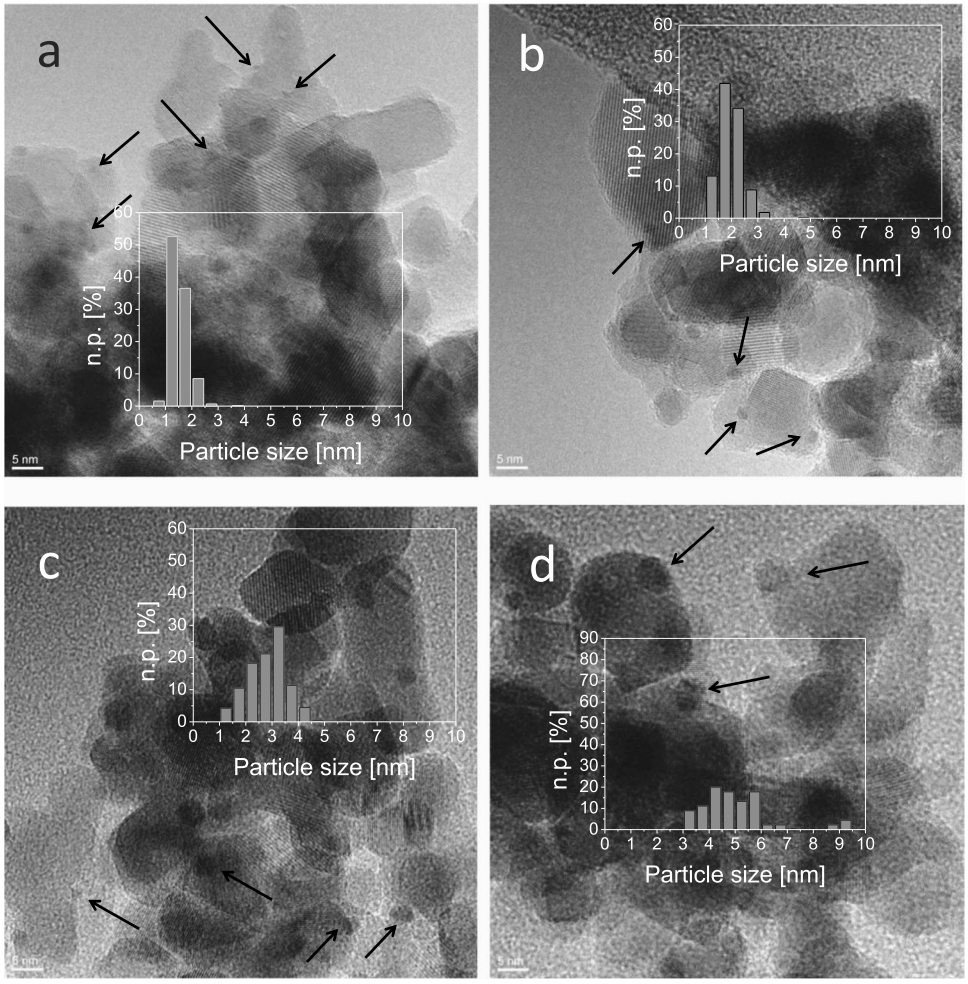

Fig. 1. HR-TEM representative images and gold particle size distribution of AuZ423 (a), AuZ573 (b), AuZ773 (c) and AZ923 (section d). Au nanoparticles are signalled by arrows. Instrumental magnification: 300000 × .

3. Results and discussion

3.1. Effect of the Au dispersion on the catalytic activity and nature of the exposed sites

The results of the HR-TEM characterization are summarized in Fig. 1, where representative images of the Au/ZrO_2 catalysts calcined at different temperatures are shown along with the corresponding particle size distributions.

Very small roundish Au particles (indicated by arrows) with average diameter of 1.5 ± 0.3 nm, which results in a Au SSA of 91.2 m^2/g, have been observed on the AuZ423 catalyst (Fig. 1, section a). Indeed, the particle size distribution is quite narrow and symmetric (see the inset in section a), which means that the Au nanoparticles are very small, having homogeneous size mainly between 1 and 2 nm. In addition, tiny gold species with size < 1 nm (0.5–0.7 nm, indicated by arrows), i.e., clusters, have been detected, too. In this frame, the presence of species even smaller in size i.e., below the detection limit of the microscope, cannot be ruled out.

The calcination at 573 K did not significantly affect the Au size and morphology (Fig. 1, section b) since an average diameter equal to d_m= 1.9 ± 0.4 nm has been obtained. Based on the particle size distribution the Au SSA is equal to 70.7 m^2/g. Again, the shape of the particle size distribution is narrow due to the presence very small particles and clusters, but it is shifted towards higher sizes. Larger Au nanoparticles with size ranging between 1.5 and 4.5 nm were detected upon calcination at 773 K, which resulted in a broader size distribution if compared to those related to AuZ423 and AuZ573. The average diameter d_m is 2.7 ± 0.7 nm, whereas the Au SSA corresponds to 48.6 m^2/g (Fig. 1, section c). Nevertheless, looking at the size distribution, the size of a large fraction (about 35%) of particles remains very small, below 2.5 nm, indicating that the calcination at high temperature did not change drastically the metal dispersion. It could be hypothesized that very small particles and, possibly, clusters still coexist together with larger particles. Conversely, the thermal treatment at 923 K has a dramatic effect on the Au size. Particles with d_m= 5.3 ± 1.6 nm have been observed along with an increase in size of zirconia particles (Fig. 1, section d), while the Au size distribution extends in the size range between 3 and 9 nm, with the disappearance of small particles and clusters, which leads to a Au SSA corresponding to 26.5 m^2/g.

The as prepared catalysts, i.e. after final calcination during the preparation are differently coloured and DR UV-Vis-NIR analysis (Figure SM-1) revealed that position, shape, and intensity of the Au plasmonic bands [40] depend on the particle size detected by HR-TEM. The red shift of the plasmon band indicates that the size of the synthesized gold particles increased [41] by increasing the calcination temperature. Moreover, the broad absorption in the 20000–41000 cm^{-1} interval increases in intensity by increasing the calcination temperature and could be likely due to the presence of residual Au^+ and/or Au^{3+} species which are not reduced upon increase of the calcination temperature [42]. Indeed, such species have been observed also on AuZ773 and AuZ923. It is worth noting that, as for these catalysts, the intensity of the bands assigned to oxidized Au appears higher than that observed for AuZ423 and AuZ573 because of the simultaneous increase in intensity of the plasmonic absorption. To further confirm this assignment, DR UV-Vis--NIR spectra in controlled atmosphere and temperature have been collected on the AuZ423 and AuZ923 catalysts after reduction (the samples were previously submitted to deg./ox. 423 or 673 K, respectively and then red./deg. 423 K, see details of the activation procedure in Table SM-1). As show in Figure SM-1, sections b and c, the comparison in the 41000–20000 cm^{-1} range between the spectra of the as prepared (full line) and reduced (dashed line) AuZ423 and AuZ923 catalysts reveals that the bands due to the oxidized species are depleted indicating that they are fully reduced only upon reduction in H_2.

In section a of Fig. 2, the conversion of 2-FA after 15 min of reaction with respect to the Au SSA is shown. After 15 min reaction the conversion achieved by AuZ423, AuZ573 and AuZ773 ranges between 25% and 35%, whilst AuZ923 reached 12% conversion. A similar trend is obtained by considering the results obtained when both 2-FA conversion and selectivity to methylfuroate are plotted with respect to the Au mean size of the different catalysts (section b). Conversion and selectivity were achieved after 180 min reaction at 393 K, 12 bar O_2 according to a previous optimization [35]. The catalysts calcined at 423, 573 and 773 K gave similar results and show very good conversion and selectivity as already observed [35].

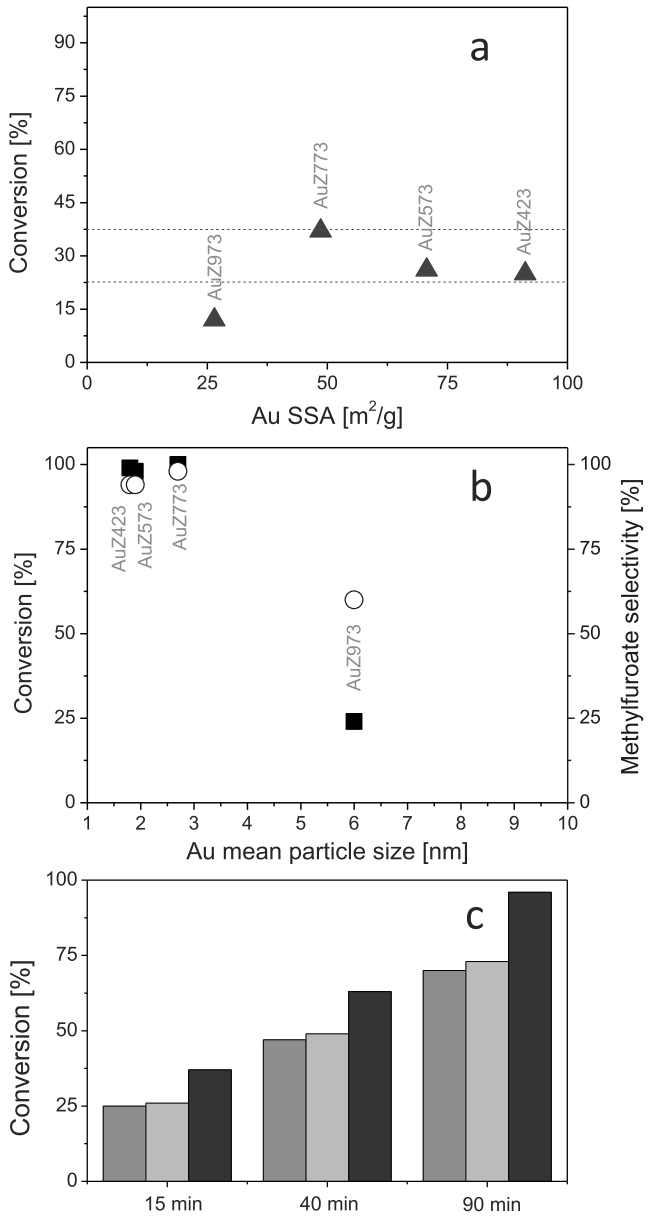

Fig. 2. Catalytic conversion after 15 min reaction at 393 K, 12 bar O_2 vs. the Au SSA calculated basing on the HR-TEM particle size distributions. The red dashed lines highlight the positions of 20% and 35% conversion (section a). Catalytic conversion (■) and selectivity to methylfuroate (○) after 180 min reaction at 393 K, 12 bar O_2 vs. the Au mean size obtained by HR-TEM analyses (section b). Conversion after 15, 40 and 90 min at 393 K, 12 bar O_2 for AuZ423 (violet), AuZ573 (pale violet) and AuZ773 (purple) catalysts (section c).

Catalytic tests performed at different reaction times (Fig. 2, section c) showed that conversion increases with the reaction time for all the samples, but AuZ773 is always the best performing sample. At the same time, the selectivity to methyl furoate does not vary significantly for the three catalysts (90%, 91% and 88%, respectively). As far as AuZ423 and

AuZ573 samples, HR-TEM analysis revealed narrow and symmetric particle size distributions, indicating homogeneous size mainly between 1 and 2 nm and very small particles with size of 0.5–0.7 nm.

The increase of the calcination temperature reduces the Au SSA from 91.2 to 70.7 m^2/g. On the AuZ773 catalyst very small particles and, likely, clusters still coexist together with larger particles, being the Au average size of this sample equal to 2.7 ± 0.7 nm (Au SSA= 48.6 m^2/g). Conversely, upon calcination at 923 K small particles and clusters coalesce to form large particles, as d_m= 5.3 ± 1.6 nm and Au SSA= 48.6 m^2/g. These features are accompanied by a drastic decrease in productivity and selectivity of the catalyst. Indeed, the sample calcined at 923 K displays remarkably low conversion (about 24%) and selectivity (about 60%) if compared to the other catalysts. However, if assuming that Au clusters are essential for the activity [12], the poor catalytic performances of AuZ923 cannot be explained. CO chemisorption expressed as mol_{CO}/mol_{Au} ratio provides information on gold dispersion, by giving information on the number of uncoordinated gold sites able to absorb CO [39]. The mol_{CO}/mol_{Au} ratios are much higher for AuZ243 and AuZ573 (0.651 and 0.320 mol_{CO}/mol_{Au}, respectively) further putting in evidence the presence of clusters, which expose many uncoordinated sites, and very highly dispersed species escaping from HR-TEM observation. On the contrary, the mol_{CO}/mol_{Au} ratio obtained for AuZ773 is lower (0.027), due to the simultaneous presence of small Au nanoparticles and clusters. AuZ923 possesses the lowest mol_{CO}/mol_{Au} ratio (0.009), confirming the poor dispersion because of large gold particles on these sample. Based on these findings, the nature and the relative abundance of the Au sites depending on the particle size were then investigated by FTIR spectroscopy of adsorbed CO.

In Fig. 3, section a the FTIR spectra recorded on the AuZ423 catalyst after deg./ox at 423 K and red./deg. 423 K upon the CO inlet (7.0 mbar) at 90 K and pressure reductions at the same temperature are shown in the carbonylic region. Overall, the intensity of these bands is the lowest with respect to those observed for the other catalysts due to the low activation temperature (see sections b-d and Figure SM-2). Different bands at 2090, 2145 and 2159 cm^{-1} (with a weak shoulder at 2169 cm^{-1}) were observed upon the inlet of CO at 90 K on AuZ423: the most intense one is the band at 2090 cm^{-1}. In particular, its position is red shifted with respect to the usual position at 2100 $cm^{-1}$of CO adsorbed on Au sites exposed at the surface of the metal nanoparticles [43]. Furthermore, the maximum of the band does not shift by decreasing the CO pressure, indicating that the CO molecules are not affected by lateral interactions and thus CO is adsorbed on isolated Au sites. Finally, the band does not decrease in intensity upon gradual pressure reduction to 1 mbar, indicating that the bond between CO and isolated Au sites is stable at 90 K. These observations, together with the symmetry of the band and its width and half-height (~50 cm^{-1}), and in agreement with HR-TEM and CO chemisorption results, allow to assign the band at 2090 cm^{-1} to CO adsorbed on highly dispersed Au clusters [39].

Conversely, the component at 2145 cm^{-1} decreases significantly in intensity due to the pressure decrease, indicating a weak interaction. Simultaneously with the decrease of this band, the decrease of a band at 3623 cm^{-1} in the hydroxyl region (data not shown) is observed, indicating that the component at 2145 cm^{-1} is due to CO in interaction with the OH groups of the support [44]. The band at 2159 cm^{-1}, with a weak shoulder at 2169 cm^{-1}, are assigned to CO adsorbed on different coordinatively unsaturated Zr^{4+} cations of the support [45]. Finally, the formation of weak bands in the carbonate region are observed (data not shown), indicating a low reactivity towards the formation of carbonate species.

Overall, the bands observed on AuZ573 have similar positions with respect to those observed for AuZ423, but the bands at 2170 cm^{-1} and 2150 cm^{-1} are much more intense than that at 2080 cm^{-1}, indicating that this catalyst exposes more sites related to the support, due to the higher calcination temperature that the sample underwent before the activation (deg./ox at 453 K followed by red./deg. at 423 K).

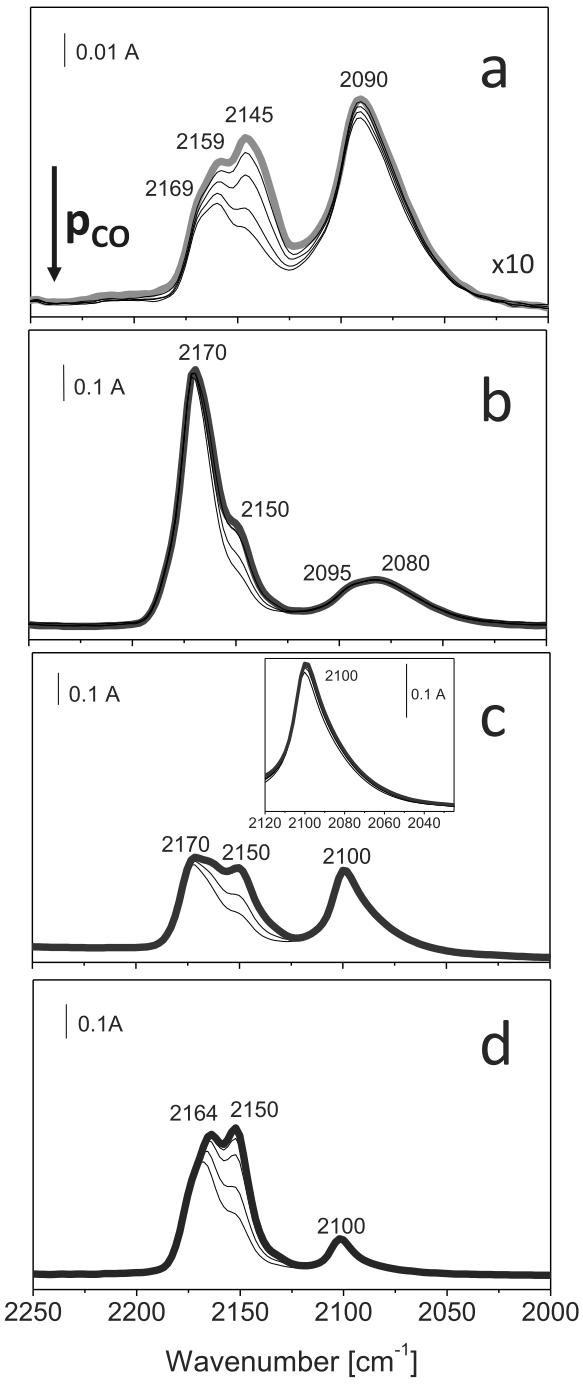

Fig. 3. FTIR Absorbance spectra collected on AuZ423 (section a), AuZ573 (section b), AuZ773 (section c) and AuZ923 (section d) after the inlet of 7.0 mbar CO at 90 K and at decreasing pressures at the same temperature. The spectra were subtracted from the spectrum of the sample before CO adsorption and are reported in the carbonyl region.

The component at 2150 cm^{-1} is related to CO in weak interaction with the OH sites of zirconia, as confirmed by its decrease following pressure reductions at the same temperature and by the decrease of absorption at 3612 cm^{-1} in the OH stretching region (see Figure SM-3).

Finally, the band at 2080 cm^{-1}, whose intensity does not change as the CO pressure decreases (pointing out stable interaction) appears broadened with respect to that related to AuZ423 and has a shoulder at 2095 cm^{-1}. It could be hypothesized that on AuZS573 a mixture of clusters (band at 2080 cm^{-1}) [46] and nanoparticles (component at 2095 cm^{-1}) [43,47] coexist, being the nanoparticles produced by

sintering of the clusters upon calcination at 423 K.

In the case of AuZ773, the bands due to CO adsorbed on Zr^{4+} (2170 cm^{-1}) and in interaction with the OH groups of the support (2150 cm^{-1}) have similar intensity than the band related to CO on Au sites (2100 cm^{-1}). This latter band is more intense, asymmetrical, and blue shifts as the CO pressure decreases (inset) due to CO lateral interactions due to the vicinity of the Au sites on the nanoparticles formed upon cluster agglomeration at 773 K. These features indicate the presence of Au corner and edge sites exposed at the surface of the nanoparticles [47].

CO adsorption on AuZ923 (section d) produced bands at 2164, 2150 and 2100 cm^{-1} related to Zr^{4+} sites, surface OH groups, and Au sites, respectively. The relative intensity among the bands is different, since the bands related to the support are much more intense than the band due to the metal. Larger particles are formed upon calcination at 923 K, affecting the size distribution of the gold particles as already revealed by HR-TEM. Analogously to AuZ773, the asymmetrical shape of the band at 2100 cm^{-1} reveals the presence of Au corner and edge sites exposed at the surface of the nanoparticles [47].

Finally, the reduction in H_2 at 423 K proved to be effective since the CO probe did not detect any oxidized gold species at the surface of the catalysts.

3.2. Reactivity of the Au sites toward molecular O_2 from 90 K up to r.t

The reactivity of the Au sites was probed by adsorbing molecular oxygen at 90 K on pre-adsorbed CO to check the capability of the catalysts to oxidize CO to CO_2 and to understand which sites are involved in oxygen activation. Section a of Fig. 4 shows the FTIR difference spectra collected on AuZ423 after the inlet of 1 mbar O_2 at 90 K on pre-adsorbed CO at increasing contact times at the same temperature in the 2400–2000 cm^{-1} range. Conversely, the evolution of the spectra in the carbonate region from 90 K up to r.t. is reported in section b.

The inlet of oxygen O_2 on pre-adsorbed CO at increasing contact times at 90 K leads to: (i) formation of a very intense band at 2339 cm^{-1}, due to molecular CO_2 adsorbed on the catalyst surface [43]. The amount of CO_2 produced already at low temperature is so large that even the CO_2 containing naturally abundant ^{13}C (band at 2274 cm^{-1}) is observed; (ii) at the same time, the band at 2090 cm^{-1} due to CO on Au clusters is slightly eroded at low frequencies, while the absorptions at 2145 cm^{-1} related to CO interacting with OH groups of the support and, at 2159 and 2169 cm^{-1} assigned to CO on different Zr^{4+} sites [45] decrease in intensity; (iii) simultaneously, in the range between 1800 and 1000 cm^{-1} an intense absorption centered at 1750 cm^{-1} is formed only upon the O_2 inlet and increases in intensity with increasing contact time (inset, from violet line to grey line). Based on the contemporaneous decrease of the carbonyls on the metal and on the support when the band at 1750 cm^{-1} starts to increase, it can be hypothesized that the related species is bonded to both a zirconium ion and a borderline Au site located at the perimeter of the clusters. In these conditions, the oxidation of the CO pre-covered surface occurs upon the inlet of O_2 facilitated the formation of this species because of electron withdrawal from the surface, favoring the formation of the bent four-electron donor carbonylic species likely on perimeter sites [48].

The bands related to CO_2 and the carbonyls on Au and on the support gradually decrease in intensity by increasing the temperature from 90 K to r.t. (not shown), whereas in the carbonate region (section b of Fig. 4) very weak bands tentatively assigned to bicarbonate-like species (labelled as bic) [13] are produced at 90 K. At r.t. these species likely convert into carbonate-like species (bands at 1640 and 1337 cm^{-1}). The narrow peak at 1169 cm^{-1} that increased in intensity at increasing contact times with O_2 at 90 K (not shown), but gradually decreases and disappears at r.t., can be associated to the formation of a superoxo O_2^- species likely adsorbed on Au [49]. The bent CO species (band at 1750 cm^{-1}) gradually decreases in intensity by increasing temperature and it is finally depleted at r.t. [48].

The same experiment performed with AuZ573 (Fig. 5) showed that the band at 2080 cm^{-1} due to CO on Au sites of clusters and nanoparticles instantaneously decreases in intensity and shifts to 2096 cm^{-1} upon the inlet of O_2 (section a). These features indicated that the low-frequency component of the band is easily eroded by O_2, pointing out that the Au clusters are extremely reactive toward oxygen and take part in the reaction already at 90 K. Moreover, the formed CO_2 (band at 2340 cm^{-1}) gradually increases with time at 90 K (Fig. 5, section a). Also in this case CO_2 is produced in such amount that a weak peak assigned to CO_2 with naturally abundant ^{13}C can be observed at 2275 cm^{-1}.

As for the 1800–1000 cm^{-1} spectral range (Fig. 5, section b), weak bands related to formate and bicarbonate species start to grow up at increasing contact times at 90 K and become well evident from 90 K to r.t. (section c). Again, the bent CO species adsorbed on the perimeter sites [48] are formed upon O_2 inlet at 90 K. However, the band at 1750 cm^{-1} gradually decreases in intensity as the temperature raises from 90 K to r.t. and at the same time, as shown in section c, formate species (labelled

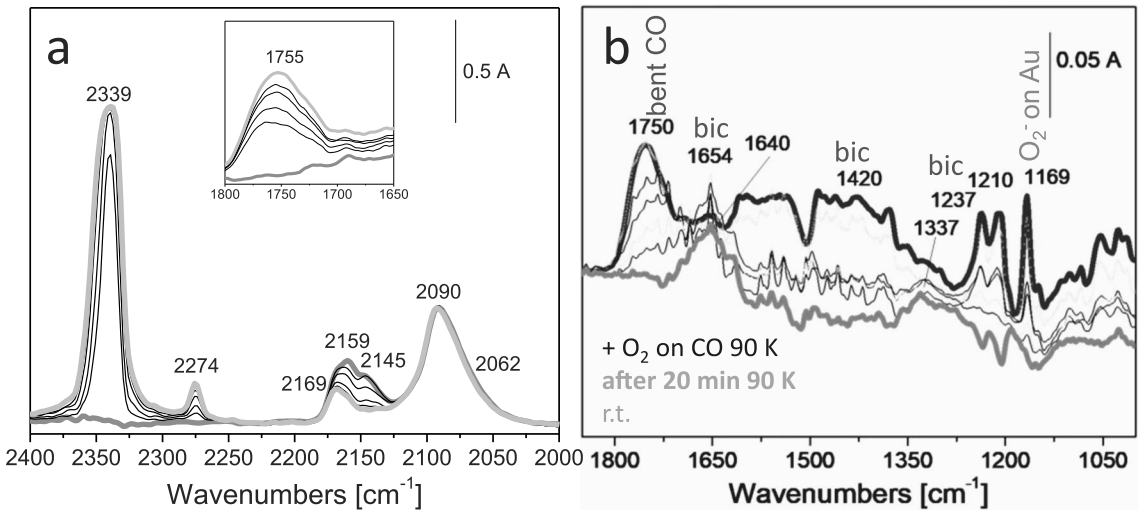

Fig. 4. FTIR Absorbance spectra collected on AuZ423 after the inlet of 1 mbar O_2 at 90 K on pre-adsorbed CO at increasing contact times (from violet line to grey line) in the 2400–2000 cm^{-1} range (section a). Evolution of the spectra in the carbonate region from 90 K (grey line) up to r.t. (violet line, section b). The spectra were subtracted from the spectrum of the sample before CO adsorption.

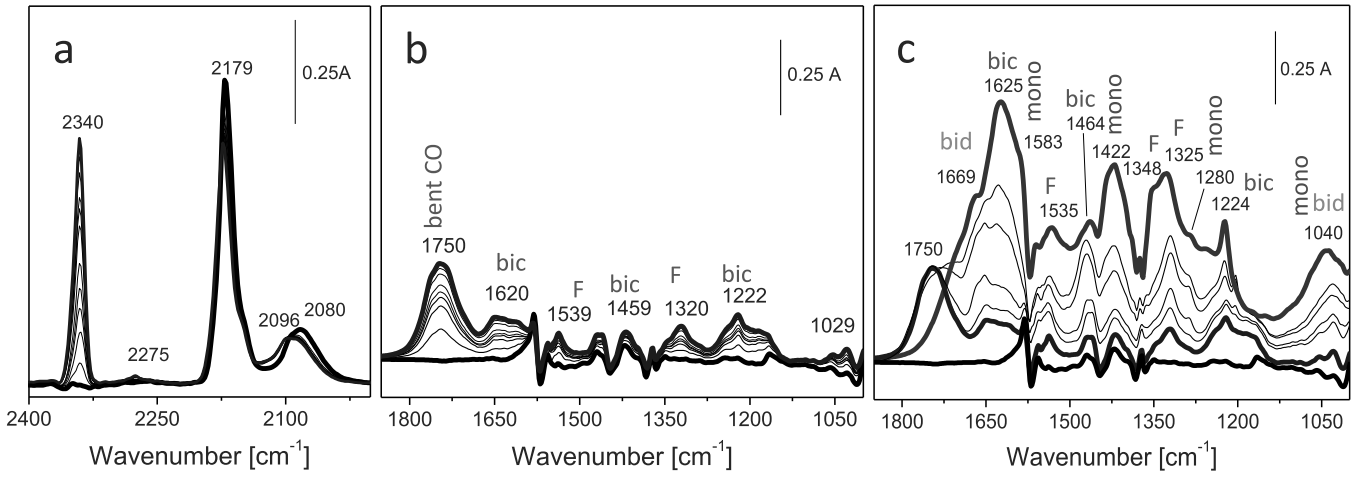

Fig. 5. FTIR Absorbance spectra collected on AuZ573 after the inlet of 1 mbar O_2 at 90 K on pre-adsorbed CO at increasing contact times (from black line to blue line) in the 2400–2000 cm^{-1} range (section a). Evolution of the spectra in the carbonate region at increasing contact times (from black line to blue line) at 90 K (section b) and from 90 K (blue line) up to r.t. (purple line, section b). The spectra were subtracted from the spectrum of the sample before CO adsorption.

as F, bands at 1535, 1348, 1325 and 2925 cm^{-1}-not shown), bicarbonate and mono- and bidentate carbonate species (labelled as bic, mono and bid) and are formed. Formates and bicarbonates are produced upon interaction between CO and CO_2 molecules with the free OH groups of the support, respectively.

The isosbestic point at 1723 cm^{-1} seems to indicate that bent CO species evolved in formate species and bicarbonate species. Mono- and bidentate carbonates are formed by interaction of the produced CO_2 with the O^{2-} sites of the support. Interestingly, no O_2^- species on Au [49] were observed on AuZ573, as a consequence of the presence of large amounts of different adsorbed species at the surface of the catalyst. Simultaneously, the increase of temperature led to the simultaneous desorption of CO and CO_2 (Figure SM-4).

Figure SM-5 shows the FTIR spectra collected after O_2 inlet at 90 K on pre-adsorbed CO at the same temperature on the AuZ773 catalyst. CO_2 is formed at 90 K also in this case, as indicated by the presence of the absorption at 2340 cm^{-1}. Either CO_2 or carbonylic bands gradually decrease in intensity until they completely disappear except for the weak absorption at 2100 cm^{-1} related to CO adsorbed on Au sites (Fig. 6, section a). At the same time, the band at 1770 cm^{-1}, due to bent CO species on the perimeter sites, has a higher intensity with respect to AuZ423 and is also blue shifted in position. The band gradually decrease in intensity upon temperature increase until it is completely depleted at r.t. (section b).

Simultaneously, the bands at 1574, 1371 and 1361 cm^{-1} ascribed to formate species produced after 20 min in the CO-O_2 atmosphere are gradually superimposed by bands at 1585, 1471, 1359 and 1015 cm^{-1} due to monodentate carbonates. Based on the behavior towards the temperature increase, the sharp peaks at 1501 and 1393 cm^{-1} (denoted with asterisks) could be assigned to transient carboxylate species [50] likely involved in the production of monodentate carbonate species. Moreover, bidentate carbonate species (bands at 1655 cm^{-1}, 1256 cm^{-1} and 1090 cm^{-1}) are observed. The sharp and intense peak at 1168 cm^{-1} is detected, which means that on this sample molecular oxygen is activated by gold particles creating also O^{2-} species on Au sites as already discussed for AuZ423. Overall, the intensity of the bands detected in the carbonate spectral region (section b) is lower than that observed for the sample calcined at 573 K. Conversely, the reactivity displayed by AuZ773 gave rise to sharp bands identifying well defined adsorbed species, according to the higher calcination temperature and the

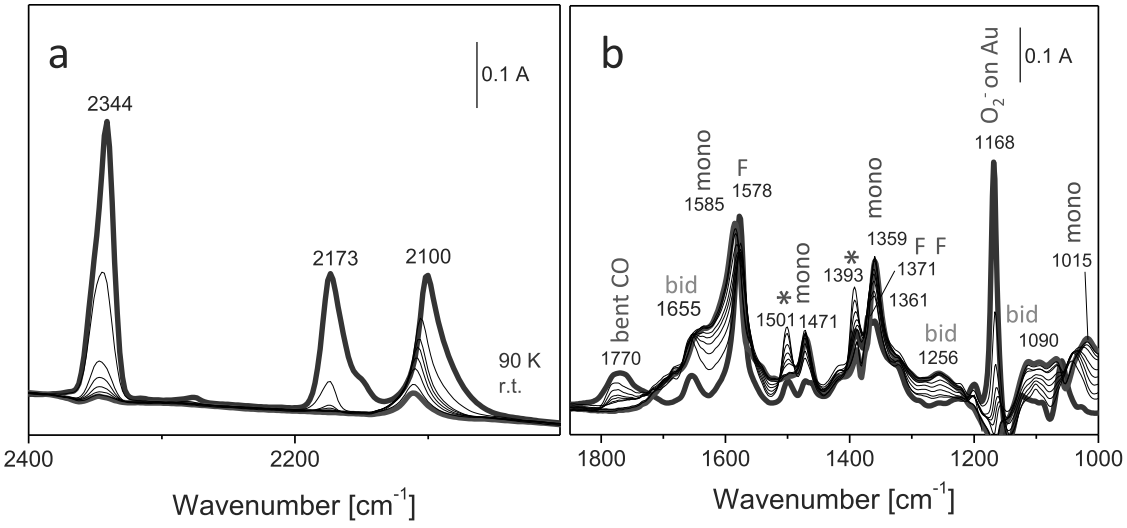

Fig. 6. FTIR Absorbance spectra collected on AuZ773 after the inlet of 1 mbar O_2 at 90 K on pre-adsorbed CO at increasing temperature from 90 K (purple line) up to r.t. (pink line) in the 2400–2000 cm^{-1} range (section a) and in the carbonate region (section b). The spectra were subtracted from the spectrum of the sample before CO adsorption.

different metal dispersion of the two catalysts.

The AuZ923 catalyst is not able to catalyze the oxidation of CO to CO_2 neither at 90 K (Figure SM-6) nor at r.t. (data not shown). The inlet of O_2 at 90 K led exclusively to the formation of the bent CO species (band at 1745 cm^{-1}), whilst formates (with bands at 1579 cm^{-1}, 1370 cm^{-1}, 1357 cm^{-1}, and 2775 cm^{-1}-not shown) already produced by CO at 90 K remain unchanged as for their intensity and position. Upon heating from 90 K up to r.t., the behavior of these bands is the same as observed for AuZ773, i.e., gradual decrease in intensity and complete erosion except for the carbonyl species on Au sites (Fig. 7, section a). In the carbonate region, the bent CO species (band at 1746 cm^{-1}) gradually decreases in intensity upon temperature increase until it is completely depleted at r.t. (section b).

Some formates are likely converted into bicarbonates (bands at 1631, 1420, 1217 cm^{-1}) and at the same time, monodentate carbonate species (bands at 1582, 1356, 1274 and 1026 cm^{-1}) are formed (section b). The superoxo O^{2-} species on Au sites (band at 1167 cm^{-1}) are observed also in this case, which points out that also the larger Au particles produced by calcination at 923 K can activate molecular oxygen.

Based on the intensity of the band of adsorbed CO_2 observed after 20 min at 90 K (Figure SM-7), that can be taken as a measure of the capability to activate O_2, the following trend can be proposed: AuZ573 > AuZ773 > AuZ423 > > AuZ923. The AuZ573 catalyst is characterized by the presence of nanoparticles and clusters. On one hand, as for AuZ773, the band related to CO on Au (2100 cm^{-1}) is higher in intensity if compared to that of AuZ573, hence exposing more Au sites. However, AuZ773 is less reactive indicating that the clusters are responsible for the better performance of AuZ573. On the other hand, AuZ423 is characterized by the presence clusters with reactivity that seems lower than that of the clusters on AuZ573. It can be proposed that because of the lower calcination temperature to which AuZ423 was submitted, the presence of residual OH groups is preventing CO from adsorption on the zirconia surface as supported by the lowest intensity of the band at 1746 cm^{-1} and that most of the produced CO_2 is probably not adsorbed.

Overall, these results indicate that the Au sites of the clusters could promote the dissociation of molecular O_2 producing atomic oxygen species, essential for the 2-FA oxidative esterification. It has been reported that on noble metals (Cu, Ag, and Au) atomically adsorbed O acts as a Brønsted base, and reactants can donate H to the O, or to adsorbed OH or alkoxides [51–54]. It is worth stressing that in our experimental conditions the 2-FA oxidative esterification is carried out without any base and in the presence of Au/ZrO_2 catalysts. Therefore, O can largely enhance the reactivity of Au surfaces toward alcohols, and it has been reported that adsorbed O is necessary to break the O−H bond and initiate the reaction, and even that Au surfaces without O are inert toward alcohols [55]. Although additional factors may be involved in O_2 activation at low temperature on oxide-supported Au catalysts, it was shown that the presence of steps and tensile strength, such as those likely occurring on highly dispersed gold species, promote O_2 adsorption and dissociation on Au [56]. Trying to get experimental evidence to support this hypothesis, DR UV-Vis spectra were collected upon the inlet of O_2 at r.t. at increasing contact time on reduced AuZ423 (violet line) and AuZ923 (blue line) catalysts and the results are shown in Figure SM-8. After 30 min upon the inlet of O_2 at r.t., an erosion of the plasmonic band is observed in both spectra (red line and orange line, respectively). Such erosion points out a modification of the electronic properties of the nanoparticles, likely due to the oxidation of a fraction of Au atoms contributing to the plasmonic collective oscillation of electrons. This feature can be taken as an indication that molecular oxygen is dissociated to atomic oxygen. Moreover, the erosion is more evident in the case of AuZ423 with respect to AuZ923, which could imply that Au clusters are more efficient than nanoparticles in molecular oxygen dissociation.

Furthermore, the FTIR CO-O_2 spectra indicate that (i) the O_2^- peroxo species can be produced also by Au nanoparticles and (ii) as a consequence, the reactivity towards O_2 appears strictly connected with the abundance of Au perimeter sites (the higher the Au size the higher their number) as revealed by the intensity of the band related to bent CO species at the perimeter between gold and the support. These species are actively connected with the CO_2 formation.

3.3. Influence of the structure of the sites on the interaction with alcohols

This section shows how the CO probe can be employed to obtain indirect information on the availability of Au sites after methanol interaction, by comparing the FTIR CO spectra before and after alcohol exposure. In these experimental conditions, methanol must be considered as a probe, not as a reactant. Moreover, no competition between methanol and CO is observed, since the methanol inlet was followed by degassing at r.t. to remove the gas phase. All the samples were submitted to reduction in H_2 at 423 K and to pre-hydration at r.t. to eliminate the contribution of the support sites and to focus on the reactivity of Au sites.

Fig. 8 shows the comparison between the spectrum collected on AuZ423 deg./ox. at 423 K then red./deg. at 423 K and previously hydrated at r.t., after CO adsorption at 90 K (blue curve) and the spectrum taken on the same sample after further interaction with CH_3OH at r.t. and subsequent CO inlet at low temperature (red curve).

CO adsorption at 90 K gives rise to a peak centered at 2150 cm^{-1}

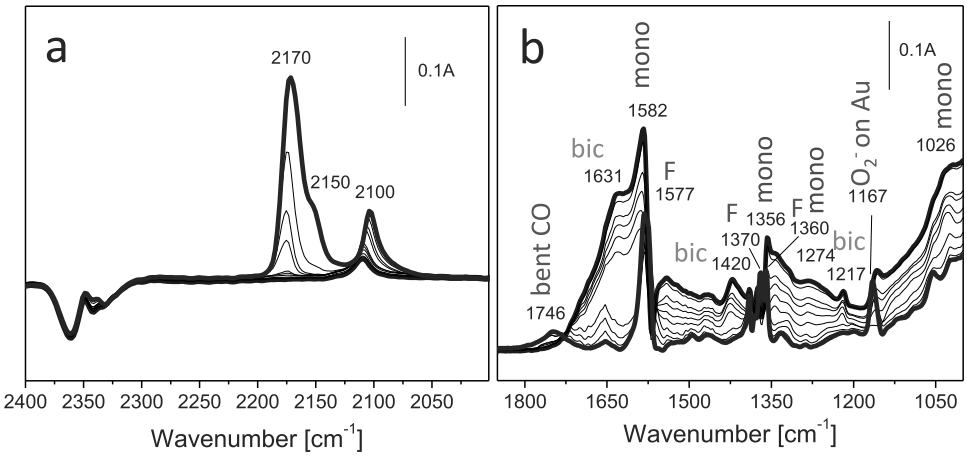

Fig. 7. FTIR Absorbance spectra collected on AuZ923 after the inlet of 1 mbar O_2 at 90 K on pre-adsorbed CO at increasing temperature from 90 K (wine line) up to r.t. (blue line) in the 2400–2000 cm^{-1} range (section a) and in the carbonate region (section b). The spectra were subtracted from the spectrum of the sample before CO adsorption.

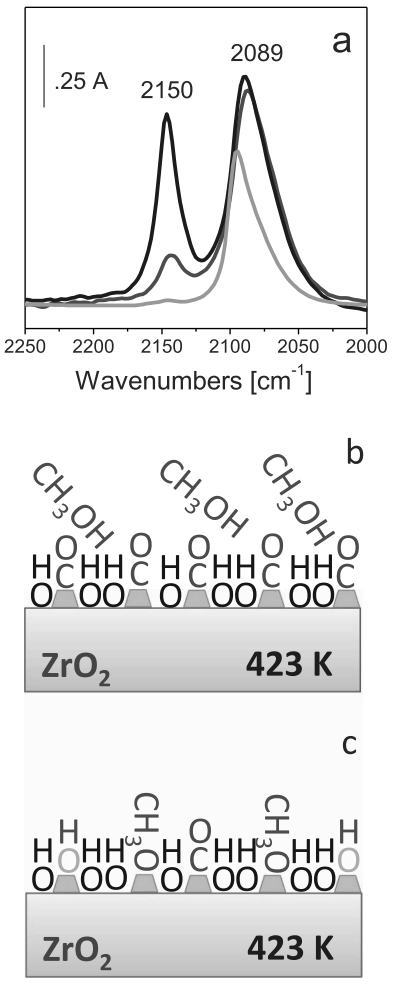

Fig. 8. Comparison among the spectrum collected upon CO (0.5 mbar) adsorption at 90 K on AuZ423 (section a) previously hydrated (0.025 mbar H_2O) at r.t. (blue curve), the spectrum taken after further interaction with CH_3OH (0.025 mbar) at r.t. and subsequent CO (0.5 mbar) inlet at 90 K (red curve) and the spectrum recorded after interaction with O_2 (50 mbar) at r.t. followed by CH_3OH (0.025 mbar) at r.t. and subsequent CO (0.5 mbar) inlet at 90 K (orange curve). Schematic representation of CO adsorption on the sample after H_2O and CH_3OH interaction (section b) and after H_2O, O_2 and CH_3OH interaction (section c).

related to CO weakly interacting with OH groups formed upon water adsorption and to a at 2089 cm^{-1} due to CO adsorbed on highly dispersed gold clusters [46] (section a, blue curve). The subsequent inlet of CO after adsorption of methanol at r.t. and cooling down to 90 K (red curve) produces a marked decrease of the band related to CO in interaction with OH groups of the support, whereas the band related to CO adsorbed on the gold sites is in the same position and with almost unchanged intensity. These spectroscopic features indicate that on AuZ423 methanol interacts with the OH groups of the support without dissociating on gold clusters, as illustrated in section b of Fig. 8.

The same experiment performed on reduced and pre-hydrated AuZ573 is reported in Fig. 9 (section a, blue curve) and reveals the same CO interaction with OH sites (band at 2150 cm^{-1}) as well as the presence of a weak component at 2161 cm^{-1} due to CO on Zr^{4+} sites. Both these features are almost depleted upon methanol adsorption (section a, red curve). The presence of some residual sites of the support after the pre-hydration procedure is reasonably because on this sample the gold nanoparticles occupy a minor fraction of support sites than highly dispersed gold clusters on AuZ423. Therefore, given the same amount of water, the sample calcined at 573 K is in some extent less hydrated than the one calcined at 423 K. This effect is further enhanced on the sample calcined at 923 K, where the gold size is the largest (see blue curve of Fig. 9, section b). Moreover, a band at 2093 cm^{-1}, with a component at lower frequencies, is observed on AuZ573 (section a, red curve) and it is assigned to CO on Au corner and edge sites exposed at the surface of the nanoparticles [47]. This band decreases in intensity after methanol interaction and a new component at 2075 cm^{-1} is observed. Beside the same observations as for the sites at higher frequencies, the decrease in intensity of the band related to CO on gold nanoparticles (band at 2098 cm^{-1}) after interaction with methanol is further pointed out on the sample calcined at 923 K (section b, red curve).

If considering that differently gold species are present on the catalysts depending on the calcination temperature, it seems quite unexpected that in the case of the AuZ423 catalyst, that is exposing quite reactive dispersed gold clusters which would be easily covered by any adsorbing molecule, the band due to CO on gold sites is practically unchanged after interaction with methanol at r.t. (Fig. 8, red curve in section a), whilst the same band decreases with increasing the size of gold species supported on zirconia (Fig. 9, red curve in sections a and b). Akita et al. [57] previously investigated the structure of the perimeters and of the contact interfaces of supported gold nanoparticles stressing on the importance of these sites as the active sites in many reactions.

Moreover, theoretical studies stressed on the importance of the presence of interfacial sites in CO oxidation [58] and methanol decomposition [59]. It was reported that methoxy species are formed at the interface between the gold and the oxide.

Due to the high dispersion, it can be assumed that the gold clusters present on AuZ423 are exposing only interfacial sites whilst the support sites are totally covered by water. In our experimental conditions, the interfacial sites are blocked by interaction with water and therefore methanol dissociation cannot take place, explaining the fact that the band at 2089 cm^{-1} remained unperturbed after methanol interaction (see section b of Fig. 8, where a schematic representation is provided). On the contrary, the decrease of the band due to CO on gold indicates that methanol activation takes place on the other two catalysts on which gold nanoparticles with larger size as well as residual support sites have been detected (the corresponding situations at the surface are reported in sections c and d of Fig. 9). Nanoparticles, beside corner and edge sites, expose also interfacial/perimeter sites, where different amounts of methoxy species are formed upon methanol interaction at r.t. as demonstrated in Figure SM-9, where a comparison among the spectra collected after methanol adsorption on the zirconia samples calcined at 573 and 973 K is shown. The shoulder at 2075 cm^{-1} observed upon methanol interaction on AuZ573 can be tentatively assigned to CO adsorbed on gold sites, possibly close to the interface with the support, where methoxy species are adsorbed, as illustrated section b of Fig. 9. This perturbation does not occur when considering the sample calcined at 923 K where the gold particles have larger size and the gold adsorbing sites are less close to each other, as indicated by the absence of the component at 2075 cm^{-1}.

Therefore, methanol can be dissociated on pre-hydrated Au/ZrO_2 catalysts strongly depending on the size of gold species and on the availability of interface sites. In the case of pre-hydrated AuZ423, where only highly dispersed gold clusters are available for CO adsorption and the interface sites are blocked by water, no methanol dissociation occurs. On this sample, the same experiment has been further repeated in the presence of oxygen when methanol inlet was performed. The CO absorption band (Fig. 8, section a, orange curve) is clearly decreased in intensity i.e., depleted from the low frequency side, if compared to the CO band obtained on the pre-hydrated sample (blue curve), indicating that the gold sites are hindered to CO adsorption possibly by methoxy species. Therefore, methanol dissociation can take place on the gold clusters covered by atomic oxygen when no metal oxide support sites are available to the adsorption. These sites favour methanol activation due to adsorbed atomic O species able to abstract H from methanol and simultaneously methoxy species, presumably on gold sites, are produced

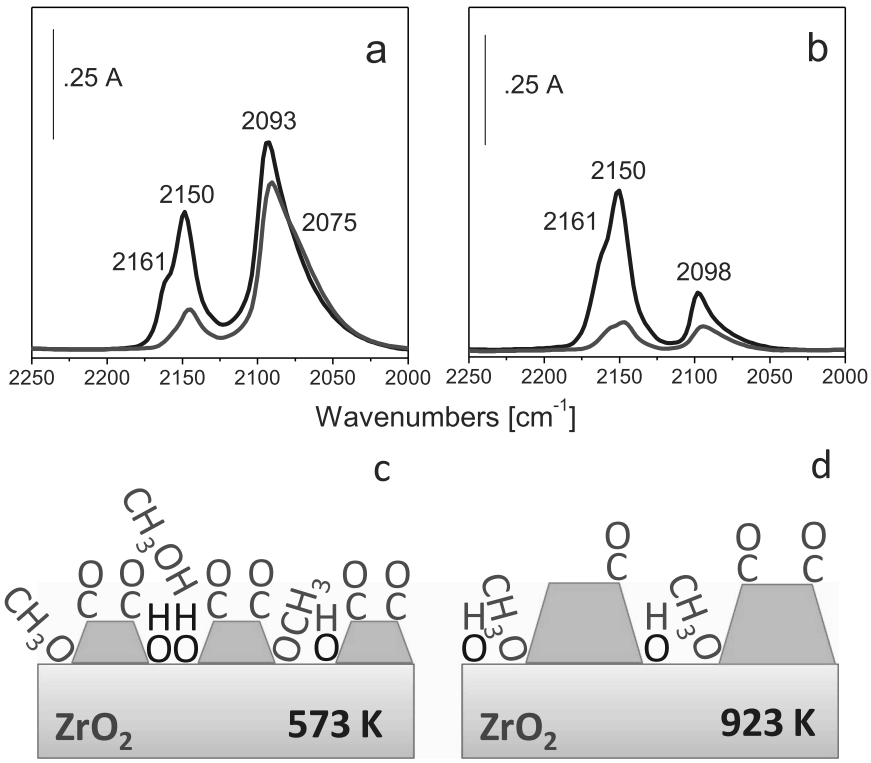

Fig. 9. Comparison between the spectrum collected upon CO (0.5 mbar) adsorption at 90 K on AuZ573 (section a) and AuZ923 (section b) previously hydrated (0.025 mbar H_2O) at r.t. (blue curve) and the spectrum taken after further interaction with CH_3OH (0.025 mbar) at r.t. and subsequent CO (0.5 mbar) inlet at 90 K (red curve). Schematic representation of CO adsorption on AuZ573 (section c) and AuZ923 (section d) after H_2O and CH_3OH interaction.

[60] (see Figure SM-10). The findings here discussed indicate that, in these experimental conditions, gold clusters behave similarly to unsupported gold nanoclusters formed upon oxidation of the Au(111) surface by ozone [61,62].

3.4. *Proposed mechanism of 2-FA esterification with molecular oxygen and methanol*

Basing on the IR spectroscopic findings, mainly corroborated by DR UV-Vis-NIR spectroscopy and HR-TEM results, a possible mechanism of 2-FA oxidative esterification to methyl 2-furoate can be proposed. Firstly, FTIR experiments carried out to investigate the CO-O_2 interaction from 90 K up to r.t. revealed that Au clusters can activate molecular O_2 to form atomic oxygen species able to promote methanol activation (Scheme 1, section a). Moreover, except for AuZ573 where large amounts of formates, bicarbonates and mono- and bidentate carbonates were produced, both clusters and nanoparticles are able to form peroxo O_2^- species (section a).

Interestingly, bent CO species (band at 1750–1770 cm^{-1}) are formed by oxygen inlet on preabsorbed CO at the perimeter between gold and zirconia. These perimeter sites can activate methanol during the 2-FA esterification reaction, since beside some linear methoxy spectator species produced on the support upon methanol inlet, methoxy species (intense band around 1160 cm^{-1}) are formed also at the Au perimeter sites by involving atomic O adsorbed on Au, as demonstrated in the case of pre-hydrated AuZ423 (Scheme 1, section b). Furthermore, it was found that furfural is adsorbed on the catalysts' surface by its carbonyl group [14]. FTIR experiments carried out at r.r. upon CO adsorption on AuZ573 red./deg. 423 K before and after 2-FA interaction (Figure SM-11) clearly put in evidence that such molecule is adsorbed on the Zr^{4+} sites of the support (Scheme 1 section c), as testified by the depletion of the CO band at 2164 cm^{-1} after interaction with furfural (section b of Figure SM-11). On the contrary, the band at 2100 cm^{-1} related to CO adsorbed Au sites is practically unchanged as for both position and shape upon furfural adsorption. Indeed, an increase in intensity of the band is even observed, due to a larger amount of CO adsorbed on these sites, because the support sites are blocked by adsorbed furfural and did not contribute to CO adsorption anymore.

Methoxy species on perimeter sites then react with adsorbed 2-FA to form methyl 2-furoate (Scheme 1, section d). A schematic representation of the 2-FA oxidative esterification to methyl 2-furoate is reported in Scheme 1.

4. Conclusions

Au/ZrO_2 catalysts with the same gold loading, but with size modulated by the final calcination temperature during preparation were tested in the 2-FA oxidative esterification under previously optimized conditions to investigate the nature of the Au sites depending on the particle size and to have information on the sites involved in the reaction, i.e. in both oxygen and methanol activation. FTIR spectroscopy of adsorbed CO, O_2 and methanol synergically coupled with HR-TEM analysis, CO chemisorption and DR-UV Vis spectroscopy have been employed to characterize the catalysts. A detailed analysis of the CO bands collected at different temperature and of the modification induced by co-interaction with oxygen, methanol and water has been presented. The measurements were performed in well-defined experimental conditions. The reactivity towards oxygen has been evaluated by studying the CO-O_2 interaction at low temperature (90 K) up to r.t. either on the catalysts containing clusters or on the samples exposing larger nanoparticles. It was found that Au clusters can activate molecular O_2 to form atomic oxygen, whereas peroxo O_2^- species were observed when either clusters or nanoparticles were present, except for AuZ573. In the absence of a base, atomic oxygen promotes methanol activation. Moreover, upon oxygen inlet, bent CO species at the perimeter between gold and the support are produced. The spectroscopic approach has been effectively employed to investigate the active gold surface sites and to put in evidence the key role displayed by these Au perimeter sites in

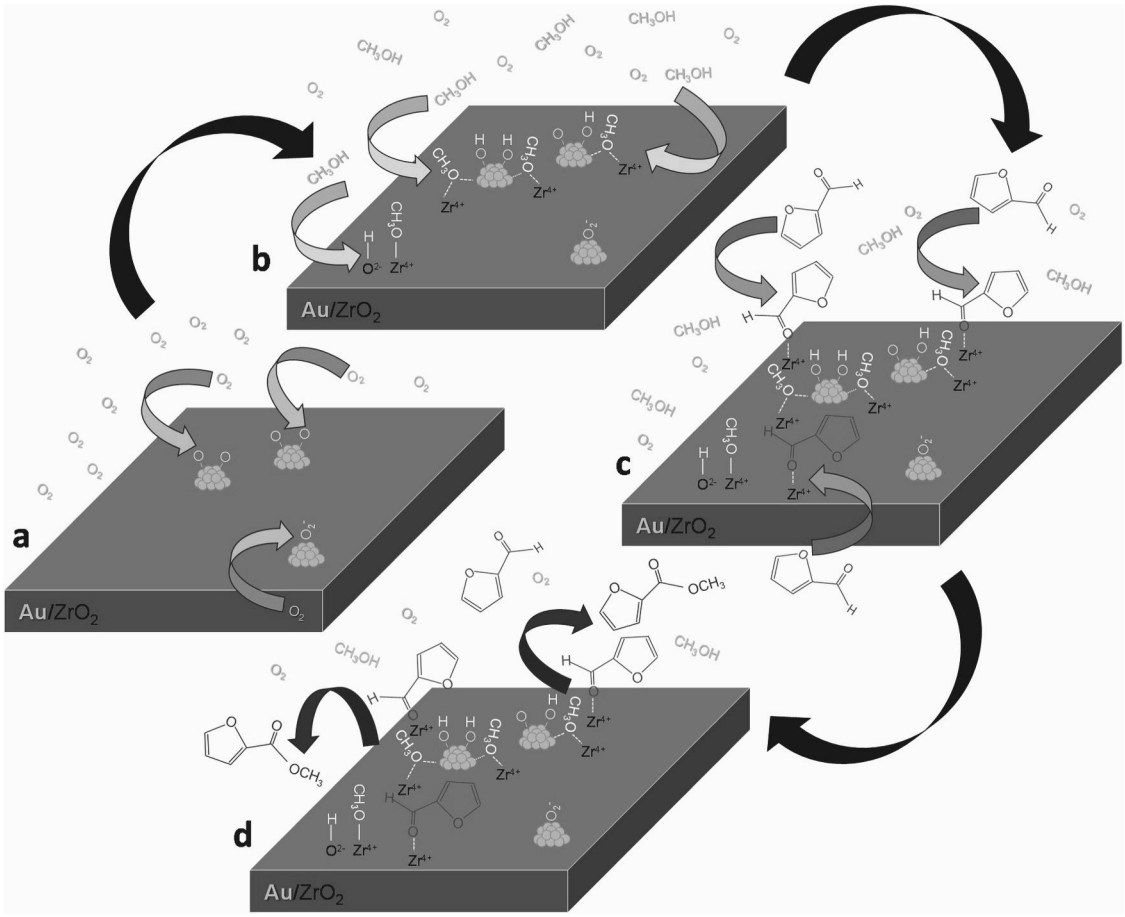

Scheme 1. Schematic representation of the 2-FA esterification to methyl 2-furoate.

methanol activation during the 2-FA esterification reaction. CO-methanol co-adsorption experiments on the pre-hydrated catalysts allowed to have information on the role of the Au sites on methanol activation, that is a reactant in the furfural esterification reaction. It has been demonstrated that methoxy species are formed on gold perimeter sites by involving an oxygen atom of the zirconia support (or atomic O adsorbed on Au as in the case of pre-hydrated AuZ423). It has been shown that furfural interacts with the catalyst's surface mainly by its carbonyl group and is adsorbed on the Zr^{4+} sites of the support and then reacts with methoxy species adsorbed on the perimeter sites. Indeed, methanol activation does not occur if such kind of sites are not available at the surface of the catalyst, indicating that in our experimental conditions highly dispersed gold clusters exhibit similar behavior to unsupported gold clusters produced on Au(111) surfaces. Finally, methyl 2-furoate is formed upon reaction between these methoxy species with adsorbed 2-FA.

Catalyst design is strategic to improve atom and energy efficiency, especially for industrial applications. These results allowed to unravel the nature and chemical environment of the Au sites at the perimeter with the support and put in evidence key role of these sites in the reaction, opening new perspectives on the design and synthesis of more performant and stable materials.

Declaration of Competing Interest

The authors declare that they have no known competing financial interests or personal relationships that could have appeared to influence the work reported in this paper.

Acknowledgement

M. M., M. B., E. C. G. and S. T. gratefully acknowledge the University of Turin (Ricerca Locale 2023) for the financial support.

Appendix A. Supporting information

Supplementary data associated with this article can be found in the online version at doi:10.1016/j.nxmate.2023.100094.

References

[1] C.H. Zhou, J.N. Beltramini, Y.X. Fan, G.Q. Lu, Chemoselective catalytic conversion of glycerol as a biorenewable source to valuable commodity chemicals, Chem. Soc. Rev. 37 (2008) 527–549, https://doi.org/10.1039/B707343G.
[2] M.J. Climent, A. Corma, S. Iborra, Conversion of biomass platform molecules into fuel additives and liquid hydrocarbon fuels, Green. Chem. 16 (2014) 516–547, https://doi.org/10.1039/C3GC41492B.
[3] J.J. Bozell, G.R. Petersen, Technology development for the production of biobased products from biorefinery carbohydrates—the US Department of Energy's "Top 10″ revisited, Green. Chem. 12 (2010) 539–554, https://doi.org/10.1039/B922014C.
[4] R. Mariscal, P. Maireles Torres, M. Ojeda, I. Sadaba, M. Lopez Granados, Furfural: a renewable and versatile platform molecule for the synthesis of chemicals and fuels, Energy Environ. Sci. 9 (2016) 1144–1189, https://doi.org/10.1039/C5EE02666K.
[5] Furfural Derivatives Market – Global Industry Analysis, Size, Share, Growth Trends, and Forecast 2016–2024, Transparency Market Research, 2016.
[6] J. Yang, N. Li, S. Li, W. Wang, L. Li, A. Wang, X. Wang, Y. Cong, T. Zhang, Synthesis of diesel and jet fuel range alkanes with furfural and ketones from lignocellulose under solvent free conditions, Green. Chem. 16 (2014) 4879–4884, https://doi.org/10.1039/C4GC01314J.
[7] A. Escobar, M. Perez, A. Sathicq, M. García, A. Paola, G. Romanelli, G. Blustein, Alkyl 2-furoates obtained by green chemistry procedures as suitable new antifoulants for marine protective coatings, J. Coat. Technol. Res. 16 (2019) 159–166, https://doi.org/10.1007/s11998-018-0110-3.
[8] E. Taarning, I.S. Nielsen, K. Egeblad, R. Madsen, C.H. Christensen, Chemicals from renewables: aerobic oxidation of furfural and hydroxymethylfurfural over gold

catalysts, ChemSusChem 1 (2008) 75–78, https://doi.org/10.1002/cssc.200700033.
[9] X. Tong, Z. Liu, L. Yu, Y. Li, A tunable process: catalytic transformation of renewable furfural with aliphatic alcohols in the presence of molecular oxygen, Chem. Commun. 51 (2015) 3674–3677, https://doi.org/10.1039/C4CC09562F.
[10] C. P. Ferraz, A.H. Braga, M.N. Ghazzal, M. Zielinski, M. Pietrowski, I. Itabaiana, F. Dumeignil, L.M. Rossi, R. Wojcieszak, Efficient oxidative esterification of furfural using Au nanoparticles supported on group 2 alkaline earth metal oxides, Catalysts 10 (2020) 430, https://doi.org/10.3390/CATAL10040430.
[11] M. Manzoli, F. Menegazzo, M. Signoretto, D. Marchese, Biomass derived chemicals: furfural oxidative esterification to methyl-2-furoate over gold catalysts, Catalysts 6 (2016) 107, https://doi.org/10.3390/CATAL6070107.
[12] F. Pinna, A. Olivo, V. Trevisan, F. Menegazzo, M. Signoretto, M. Manzoli, F. Boccuzzi, The effects of gold nanosize for the exploitation of furfural by selective oxidation, Catal. Today 203 (2013) 196–201, https://doi.org/10.1016/j.cattod.2012.01.033.
[13] F. Menegazzo, M. Signoretto, F. Pinna, M. Manzoli, V. Aina, G. Cerrato, F. Boccuzzi, Oxidative esterification of renewable furfural on gold-based catalysts: Which is the best support? J. Catal. 309 (2014) 2, https://doi.org/10.1016/j.jcat.2013.10.005.
[14] F. Menegazzo, T. Fantinel, M. Signoretto, F. Pinna, M. Manzoli, On the process for furfural and HMF oxidative esterification over Au/ZrO_2, J. Catal. 319 (2014) 61–70, https://doi.org/10.1016/j.jcat.2014.07.017.
[15] O. Casanova, S. Iborra, A. Corma, Biomass into chemicals: One pot-base free oxidative esterification of 5-hydroxymethyl-2-furfural into 2,5-dimethylfuroate with gold on nanoparticulated ceria, J. Catal. 265 (2009) 109–116, https://doi.org/10.1016/j.jcat.2009.04.019.
[16] C. Ampelli, K. Barbera, G. Centi, C. Genovese, G. Papanikolaou, S. Perathoner, K. J. Schouten, J.K. Vander Waal, On the nature of the active sites in the selective oxidative esterification of furfural on Au/ZrO_2 catalysts, Catal. Today 278 (2016) 56–65, https://doi.org/10.1016/j.cattod.2016.04.023.
[17] C. Ampelli, K. Barbera, G. Centi, C. Genovese, G. Papanikolaou, S. Perathoner, K. J. Schouten, J.K. Vander Waal, On the nature of the active sites in the selective oxidative esterification of furfural on Au/ZrO2 catalysts, Catal. Today 278 (2016) 56–65, https://doi.org/10.1016/j.cattod.2016.04.023.
[18] C. P. Ferraz, A.H. Braga, M.N. Ghazzal, M. Zielińnski, M. Pietrowski, I. Itabaiana, F. Dumeignil, L.M. Rossi, R. Wojcieszak, Efficient oxidative esterification of furfural using Au nanoparticles supported on group 2 alkaline earth metal oxides, Catalysts 10 (2020) 430, https://doi.org/10.3390/CATAL10040430.
[19] X. Tong, Z. Liu, L. Yu, Y. Li, A tunable process: catalytic transformation of renewable furfural with aliphatic alcohols in the presence of molecular oxygen, Chem. Commun. 51 (2015) 3674–3677, https://doi.org/10.1039/C4CC09562F.
[20] Y. Feng, S. Long, G. Yan, W. Jia, Y. Sun, X. Tang, Z. Zhang, X. Zeng, L. Lin, Highly dispersed Co/N-rich carbon nanosheets for the oxidative esterification of biomass derived alcohols: Insights into the catalytic performance and mechanism, J. Catal. 397 (2021) 148–155, https://doi.org/10.1016/J.JCAT.2021.03.031.
[21] K. Ghosh, M.A. Iqubal, R.A. Molla, A. Mishra, K. Kamaluddin, S.M. Islam, Direct oxidative esterification of alcohols and hydration of nitriles catalyzed by a reusable silver nanoparticle grafted onto mesoporous polymelamine formaldehyde (AgNPs@mPMF), Catal. Sci. Technol. 5 (3) (2015) 1606–1622, https://doi.org/10.1039/C4CY01278J.
[22] B. Wang, W. Ran, W. Sun, K. Wang, Direct oxidative esterification of aldehyde with alcohol to ester over Pd/styrene-divinyl benzene copolymer catalyst, Ind. Eng. Chem. Res. 51 (2012) 3932–3938, https://doi.org/10.1021/ie202701k.
[23] Y. Liu, X. Jiao, F. Zhang, D. Cheng, W. Qin, Efficient and selective oxidation of furfural into high-value chemicals by cobalt and nitrogen co-doped carbon, Can. J. Chem. Eng. 101 (2023) 354–367, https://doi.org/10.1002/cjce.24376.
[24] R.V. Jagadeesh, H. Junge, M.M. Pohl, J. Radnik, A. Brückner, M. Beller, Selective oxidation of alcohols to esters using heterogeneous Co3O4-N@C catalysts under mild conditions, J. Am. Chem. Soc. 135 (2013) 10776–10782, https://doi.org/10.1021/ja403615c.
[25] Z. Liu, X. Tong, J. Liu, S. Xue, A smart catalyst system for the valorization of renewable furfural in aliphatic alcohols, Catal. Sci. Technol. 6 (2016) 1214–1221, https://doi.org/10.1039/C5CY01195G.
[26] C. Bianchi, F. Porta, L. Prati, M. Rossi, Selective liquid phase oxidation using gold catalysts, Top. Catal. 13 (2000) 231–236, https://doi.org/10.1023/A:1009065812889.
[27] R.J. Madix, C.M. Friend, X. Liu, Anticipating catalytic oxidation reactions on gold at high pressure (including liquid phase) from ultrahigh vacuum studies, J. Catal. 258 (2008) 410–413, https://doi.org/10.1016/J.JCAT.2008.06.026.
[28] K.M. Kosuda, A. Wittstock, C.M. Friend, M. Bäumer, Oxygen-Mediated Coupling of Alcohols over Nanoporous Gold Catalysts at Ambient Pressures, Angew. Chem. Int. Ed. 51 (2012) 1698–1701, https://doi.org/10.1002/anie.201107178.
[29] B.N. Zope, D.D. Hibbitts, M. Neurock, R.J. Davis, Reactivity of the gold/water interface during selective oxidation catalysis, Science 330 (2010) 74–78, https://doi.org/10.1126/science.1195055.
[30] C.R. Chang, X.F. Yang, B. Long, J. Li, A water-promoted mechanism of alcohol oxidation on a Au(111) surface: understanding the catalytic behavior of bulk gold, ACS Catal. 3 (2013) 1693–1699, https://doi.org/10.1021/cs400344r.
[31] M. Boronat, A. Corma, F. Illas, J. Radilla, T. Rodenas, M.J. Sabater, Mechanism of selective alcohol oxidation to aldehydes on gold catalysts: Influence of surface roughness on reactivity, J. Catal. 278 (2011) 50–58, https://doi.org/10.1016/J.JCAT.2010.11.013.
[32] K. Kaehler, M.C. Holz, M. Rohe, A.C. van Veen, M. Muhler, Methanol oxidation as probe reaction for active sites in Au/ZnO and Au/TiO_2 catalysts, J. Catal. 299 (2013) 162–170, https://doi.org/10.1016/j.jcat.2012.12.001.
[33] F. Boccuzzi, A. Chiorino, M. Manzoli, FTIR study of methanol decomposition on gold catalyst for fuel cells, J. Power Sources 118 (2003), https://doi.org/10.1016/S0378-7753(03)00075-2.
[34] M. Manzoli, A. Chiorino, F. Boccuzzi, Decomposition and combined reforming of methanol to hydrogen: A FTIR and QMS study on Cu and Au catalysts supported on ZnO and TiO_2, Appl. Catal. B 57 (2005), https://doi.org/10.1016/j.apcatb.2004.11.002.
[35] M. Signoretto, F. Menegazzo, L. Contessotto, F. Pinna, M. Manzoli, F. Boccuzzi, Au/ZrO2: an efficient and reusable catalyst for the oxidative esterification of renewable furfural, Appl. Catal. B: Env. 129 (2013) 287–293, https://doi.org/10.1016/j.apcatb.2012.09.035.
[36] M. Manzoli, F. Menegazzo, M. Signoretto, G. Cruciani, F. Pinna, Effects of synthetic parameters on the catalytic performance of Au/CeO2 for furfural oxidative esterification, J. Catal. 330 (2015) 465–473, https://doi.org/10.1016/J.JCAT.2015.07.030.
[37] A. Delparish, A.W.N. de Leeuw den Bouter, A. Yercan, J. van der Schaaf, M.F. Neira d'Angelo, Bringing the promises of microreactors and gold catalysis to lignocellulosic biomass valorization: A study on oxidative transformation of furfural, Chem. Eng. J. 452 (2023), 138903, https://doi.org/10.1016/j.cej.2022.138903.
[38] M. Manzoli, F. Boccuzzi, V. Trevisan, F. Menegazzo, M. Signoretto, F. Pinna, Au/ZrO_2 catalysts for LT-WGSR: Active role of sulfates during gold deposition, Appl. Catal. B Environ. 96 (2010), https://doi.org/10.1016/j.apcatb.2010.01.030.
[39] F. Menegazzo, F. Pinna, M. Signoretto, V. Trevisan, F. Boccuzzi, A. Chiorino, M. Manzoli, Quantitative determination of sites able to chemisorb CO on Au/ZrO_2 catalysts, Appl. Catal. A 356 (2009) 31–35, https://doi.org/10.1016/j.apcata.2008.12.004.
[40] A. Villa, N. Dimitratos, C.E. Chan-Thaw, C. Hammond, G.M. Veith, D. Wang, M. Manzoli, L. Prati, G.J. Hutchings, Characterisation of gold catalysts, Chem. Soc. Rev. 45 (2016) 4953–4994, https://doi.org/10.1039/C5CS00350D.
[41] B. Balamurugan, T. Maruyama, Appl. Phys. Lett. 87 (2005), 143105.
[42] T.M. Salama, T. Shido, R. Ohnishi, M. Ichikawa, EXAFS/XANES, XRD, and UV−Vis Characterization of Intrazeolitic Gold(I) Prepared by Monolayer Dispersion of AuCl3 inside Na−Y Zeolite, J. Phys. Chem. 100 (1996) 3688–3694, https://doi.org/10.1021/jp951996g.
[43] F. Boccuzzi, A. Chiorino, M. Manzoli, P. Lu, T. Akita, S. Ichikawa, M. Haruta, Au/TiO_2 Nanosized Samples: A Catalytic, TEM, and FTIR Study of the Effect of Calcination Temperature on the CO Oxidation, J. Catal. 202 (2001) 256–267, https://doi.org/10.1006/jcat.2001.3290.
[44] M. Manzoli, A. Chiorino, F. Boccuzzi, FTIR study of nanosized gold on ZrO_2 and TiO_2, Surf. Sci. 532–535 (2003) 377–382, https://doi.org/10.1016/S0039-6028(03)00225-5.
[45] C. Morterra, V. Bolis, B. Fubini, L. Orio, A FTIR and HREM study of some morphological and adsorptive properties of monoclinic ZrO_2 microcrystals, /252, Surf. Sci. 251 (1991) 540, https://doi.org/10.1016/0039-6028(91)91051-X.
[46] F. Menegazzo, F. Pinna, M. Signoretto, V. Trevisan, F. Boccuzzi, A. Chiorino, M. Manzoli, Highly dispersed gold on zirconia: Characterization and activity in low-temperature water gas shift tests, ChemSusChem 1 (2008) 320–326, https://doi.org/10.1002/cssc.200700152.
[47] A. Chiorino, M. Manzoli, F. Menegazzo, M. Signoretto, F. Vindigni, F. Pinna, F. Boccuzzi, New insight on the nature of catalytically active gold sites: Quantitative CO chemisorption data and analysis of FTIR spectra of adsorbed CO and of isotopic mixtures, J. Catal. 262 (2009) 169–176, https://doi.org/10.1016/j.jcat.2008.12.017.
[48] G. Ghiotti, F. Boccuzzi, A. Chiorino, Spectroscopic evidence for a new surface carbonyl species on a Cu/ZnO catalyst, J. Soc. Chem. Commun. (1985), https://doi.org/10.1039/C39850001012.
[49] A.P. Woodham, A. Fielicke, Superoxide formation on isolated cationic gold clusters, Angew. Chem. Int. Ed. 53 (2014) 6554–6557, https://doi.org/10.1002/anie.201402783.
[50] M. Manzoli, A. Chiorino, F. Boccuzzi, Interface species and effect of hydrogen on their amount in the CO oxidation on Au/ZnO, Appl. Catal. B: Environ. 52 (2004) 259–266, https://doi.org/10.1016/j.apcatb.2004.04.011.
[51] M.L. Personick, R.J. Madix, C.M. Friend, Selective oxygen-assisted reactions of alcohols and amines catalyzed by metallic gold: paradigms for the design of catalytic processes, ACS Catal. 7 (2017) 965–985.
[52] Q. Meng, Y. Shen, J. Xu, J. Gong, Mechanistic insights into selective oxidation of ethanol on Au(111): a DFT study, Chin. J. Catal. 33 (2012) 407–415.
[53] B. Xu, J. Haubrich, T.A. Baker, E. Kaxiras, C.M. Friend, Theoretical study of O-assisted selective coupling of methanol on Au(111), J. Phys. Chem. C. 115 (2011) 3703–3708.
[54] B.N. Zope, D.D. Hibbitts, M. Neurock, R.J. Davis, Reactivity of the gold/water interface during selective oxidation catalysis, Science 330 (2010) 74–78 (M.).
[55] T. Yan, J. Gong, C.B. Mullins, Oxygen exchange in the selective oxidation of 2-butanol on oxygen precovered Au(111), J. Am. Chem. Soc. 131 (2009) 16189–16194 (J.).
[56] Y. Xu, M. Mavrikakis, Adsorption and dissociation of O2 on gold surfaces: effect of steps and strain, J. Phys. Chem. B 107 (2003) 9298–9307.
[57] T. Akita, M. Kohyama, M. Haruta, Electron microscopy study of gold nanoparticles deposited on transition metal oxides, Acc. Chem. Res. 46 (2013) 1773–1782, https://doi.org/10.1021/ar300259n.
[58] I.X. Green, W.J. Tang, M. Neurock, J.T. Yates, Spectroscopic observation of dual catalytic sites during oxidation of CO on a Au/TiO2 catalyst, Science 333 (2011) 736–739, https://doi.org/10.1126/science.1207272.

[59] S. Hong, T.S. Rahman, Rationale for the higher reactivity of interfacial sites in methanol decomposition on Au13/TiO2(110), J. Am. Chem. Soc. 135 (2013) 7629–7635, https://doi.org/10.1021/ja4010738.
[60] X. Liu, C.M. Friend, Selective oxidation of cyclohexanol and 2-cyclohexen-1-ol on O/Au(111): the effect of molecular structure, Langmuir 26 (2010) 16552–16557, https://doi.org/10.1021/la1015302.
[61] B. Xu, X. Liu, J. Haubrich, R.J. Madix, C.M. Friend, Selectivity control in gold-mediated esterification of methanol, Angew. Chem. Int. Ed. 48 (2009) 4206–4209, https://doi.org/10.1002/ange.200805404.
[62] B. Xu, J. Haubrich, C.G. Freyschlag, R.J. Madix, C.M. Friend, Oxygen-assisted cross-coupling of methanol with alkyl alcohols on metallic gold, Chem. Sci. 1 (2010) 310–314, https://doi.org/10.1039/C0SC00214C.